Thermal stability and evolution of microstructures induced by He irradiation in W–TiC alloys

Xu, Q.; Ding, X.Y.; Luo, L.M.; Miyamoto, M.; Tokitani, M.; Zhang, J.; Wu, Y.C.

Nuclear Materials and Energy 15 (2018) 76–79

Contents lists available at ScienceDirect

Nuclear Materials and Energy

journal homepage: www.elsevier.com/locate/nme

Thermal stability and evolution of microstructures induced by He irradiation in W–TiC alloys

Q. Xu[a,*], X.Y. Ding[b], L.M. Luo[b], M. Miyamoto[c], M. Tokitani[d], J. Zhang[a], Y.C. Wu[b]

[a] Research Reactor Institute, Kyoto University, Osaka 590-0494, Japan
[b] School of Materials Science and Engineering, Hefei University of Technology, Hefei 230031, China
[c] Shimane University, Shimane 690-8504, Japan
[d] National Institute for Fusion Science, Gifu 509-5292, Japan

ARTICLE INFO

Keywords:
W-TiC
Thermal stability
He irradiation
He bubble

ABSTRACT

Dispersion-strengthened W alloys, W-1%TiC and W-2%TiC, were fabricated by spark plasma sintering (SPS). The thermal stabilities of the secondary-phase TiC particles and microstructures in the W alloys during thermal treatments from 100 to 1000 °C were investigated by positron annihilation techniques. The TiC particles were stable in both W–TiC alloys during the annealing process. Both alloys were irradiated by 5-keV He ions at 900 °C–1.8×10^{21} He/m^2. Compared with commercially available pure W, the formation of He bubbles was suppressed by the TiC particles in the W–TiC alloys, and the extent of suppression increased as the amount of added TiC was increased.

1. Introduction

Tungsten is advantageous for many applications due to its high melting point, thermal conductivity, sputtering resistance, and low hydrogen isotope retention. Therefore, it is a potential candidate for use in plasma-facing materials (PFMs). However, embrittlement induced by low-temperatures, recrystallization, and irradiation has prevented the widespread use of W in PFMs. To improve the mechanical properties of W, secondary-phase particles such as TiC, La_2O_3, and Y_2O_3 can be added to the W alloys. It has been reported that W–TiC alloys with ultra-fine grain size prepared by mechanical alloying (MA) have good ductility at low temperatures and good radiation resistance [1–3]. However, impurities originating from the balls and containers used in the MA process are mixed in the alloys, which adversely affect their mechanical properties. In addition, distortion induced by the MA process remains in the W alloys, increasing the possibility of cracking during sintering. To overcome this limitation, the wet-chemical method has been developed, where the raw material powder is mixed and sintered at high temperature [4]. Although the W–TiC alloys fabricated by the wet-chemical method show good mechanical properties, their resistance to irradiation has not yet been investigated sufficiently. In the present study, we investigated the effects of TiC content on the thermal stability of the microstructures in W alloys, and formation of He bubbles under He irradiation at high temperature.

2. Experimental procedure

W-1%TiC and W-2%TiC (in weight percent) alloys were fabricated by the wet-chemical method [5–7]. The surface was scraped by about 2 mm to avoid the influence of the carbonized layer on the surface of the ingots. Then, these alloys were cut into dimensions of ϕ5 mm × 0.3 mm- (thickness), and mechanically polished to a mirror-like finish for investigating the microstructure thermal stability. Isochronal annealing experiments were performed on these samples for 5 h in 100 °C increments from 25 to 1000 °C under a vacuum pressure lower than 1×10^{-4} Pa. The effects of thermal annealing on microstructural evolution in the W–TiC alloys were investigated by scanning electron microscopy (SEM) with energy dispersive spectrometry (EDS). In addition, positron annihilation spectroscopy, which is a non-destructive and powerful technique for detecting defect clusters, especially vacancy-type clusters in solid materials, was used to study the alloys. Positron annihilation lifetime measurements and coincidence Doppler broadening (CDB) measurements were performed before and after annealing. The positron annihilation lifetime measurements were used to monitor changes in defect clusters introduced by the manufacturing process during annealing. CDB measurements monitored the distribution change in the TiC nano-particles during annealing. The positron source was ^{22}Na with a diameter of 2 mm. The time resolution of the positron lifetime spectrometer was 190 ps (full-width at half-maximum, FWHM). The positron lifetime spectra were analyzed based on the two-

* Corresponding author.
E-mail address: xu@rri.kyoto-u.ac.jp (Q. Xu).

https://doi.org/10.1016/j.nme.2018.02.003
Received 28 November 2017; Received in revised form 24 January 2018; Accepted 23 February 2018
Available online 09 March 2018

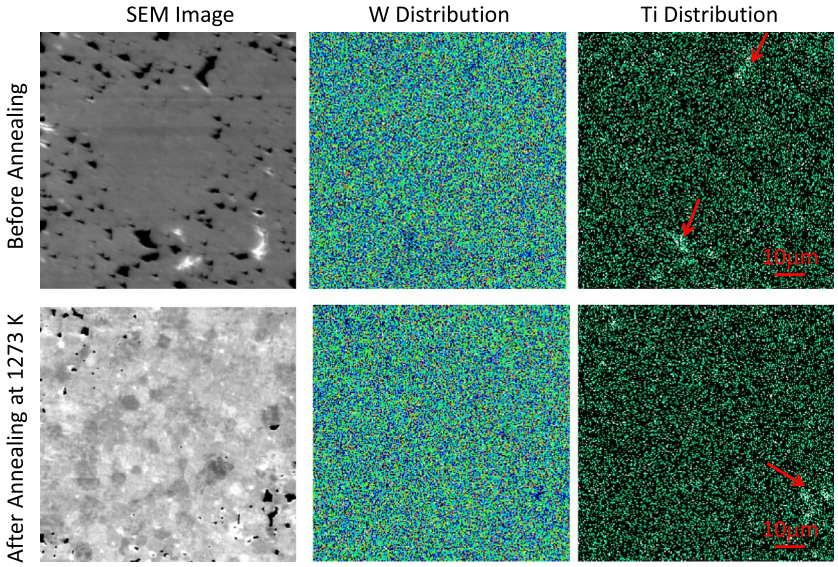

Fig. 1. SEM observations and EDX elemental analysis of the W-1%TiC alloy.

state trapping model, where the short lifetime, τ_1, corresponds to the bulk component, and the long lifetime, τ_2, corresponds to the defect component. The total count for each lifetime spectrum was over 1×10^6. The energy resolution of the CDB measurement device was 1.4 keV at 511 keV, and the total count for each CDB spectrum was over 2×10^7.

Specimens for transmission electron microscopy (TEM) observations were prepared using a focus ion beam (FIB) from the ϕ5 mm specimens. Irradiation with 5 keV He^+ ions was performed using an ion-accelerator-TEM (JEM-2010S) system installed at Shimane University. The irradiation temperature was 900 °C, and the total dose of ion irradiation was 1.8×10^{21} He/m^2 with an ion flux of 1.5×10^{18} He/m^{2}s. The damage to the substrate and He ion distributions were estimated by SRIM code [8]. The furthest damage observed was approximately 8 nm from the irradiated surface, and the damage was ~15 dpa (displacement per atom) at the peak position after irradiation to 1.8×10^{21} He/m^2. In addition, the He distribution peak was centered approximately 17 nm from the incident surface, and the concentration of He was ~0.6 at the peak position. After ion irradiation, the microstructures of the samples were observed by the same TEM system installed at Shimane University.

3. Results and discussion

Figs. 1 and 2 show the SEM images and EDS maps of W and Ti for the as-received and W alloys annealed at 1000 °C for 5 h, respectively. The black dots in the SEM images of Figs. 1 and 2 were caused by irregularities of the surface. The color represents the element, W in the W EDS map and Ti in the Ti EDS map. The TiC nano-particles were not clearly observed by SEM in the as-received or annealed W–TiC alloys. W was uniformly distributed in the as-received and annealed W–TiC samples; however, agglomerates of Ti were observed in W-1%TiC alloy, as shown by the arrows in the EDS maps. Compared with the W-1%TiC alloy, the distribution of the TiC nano-particles was more uniform in the W-2%TiC alloy. This result indicated that the stirring process in the W-1%TiC alloy fabrication was insufficient.

Fig. 3 shows the positron lifetime changes in the W–TiC alloys during annealing. The microvoid components (τ_2) were present in both the as-received W–TiC alloys, which indicated that microvoids were induced during the alloy fabrication process. The value of τ_2 was

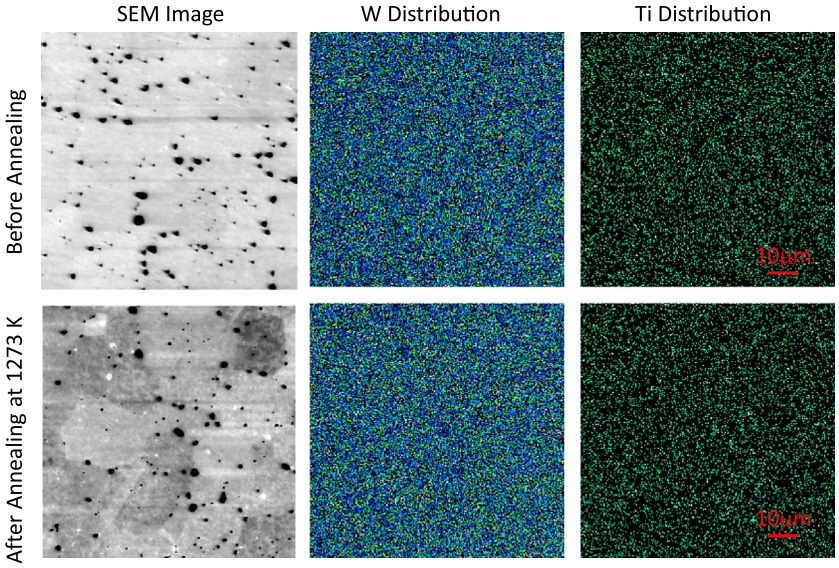

Fig. 2. SEM observations and EDX elemental analysis of the W-2%TiC alloy.

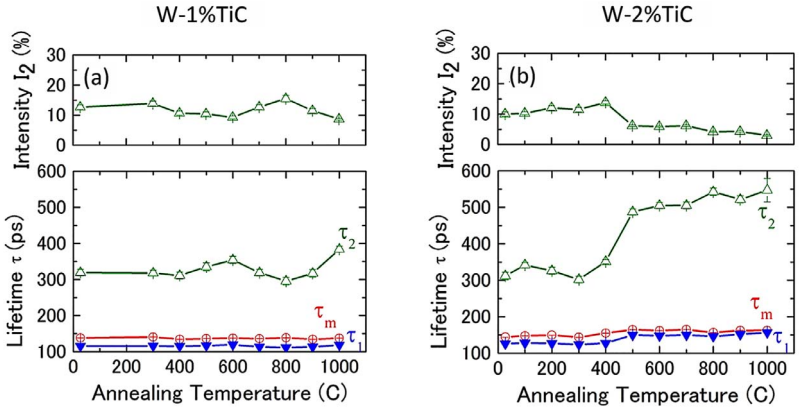

Fig. 3. Changes in the positron lifetimes and intensity of the long lifetime in the W-1%TiC (a) and W-2%TiC (b) alloys during annealing.

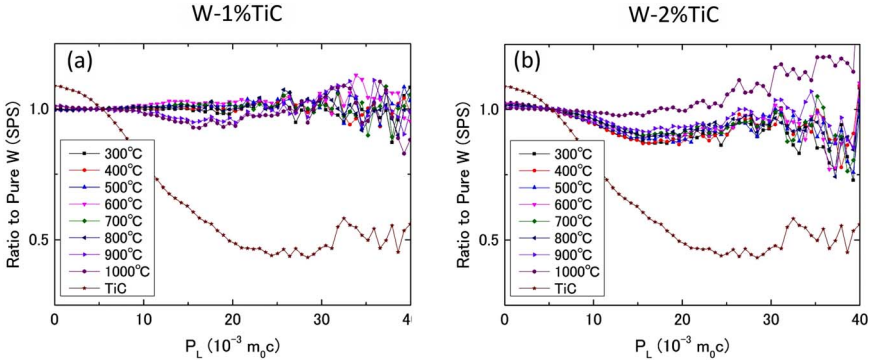

Fig. 4. Changes in the CDB curves of the W-1%TiC (a) and W-2%TiC (b) alloys during annealing.

~300 ps, which corresponds to a vacancy cluster containing seven vacancies [9]. The short lifetimes (τ_1) were 115.4 and 126 ps for the as-received W-1%TiC and W-2%TiC alloys, respectively, which correspond to the lifetime of the dislocations [10]. This result indicated that dislocations were also induced in the alloy fabrication process. During annealing at high temperatures, the long lifetimes changed significantly at 500 °C compared with those at room temperature in both W–TiC alloys. This represents the temperature at which vacancies are sufficiently mobile if the vacancy migration energy is assumed to be 1.9 eV [11] (mobility of vacancy $Mv = 10^{13}\exp(-1.9/kT)$, k: Boltzmann's constant; T: absolute temperature). The long lifetimes at temperatures higher than 500 °C in the W-2%TiC alloy were higher than those in the W-1%TiC alloy. This means the growth of microvoids was easier in the W-2%TiC alloy. Samolyuk et al. indicated that vacancy clusters containing fewer than six vacancies in pure W were unstable according to the simulations based on first principles [12]. TiC nano-particles may stabilize the vacancy clusters containing fewer than six vacancies. Therefore, it is possible that the density of tiny vacancy clusters containing fewer than six vacancies in the W-2%TiC alloy was higher than that in the W-1%TiC alloy. During annealing at temperatures higher than 500 °C, these tiny vacancy clusters were untrapped from the TiC nano-particles and dissolved to become mobile, the large microvoids absorbed these vacancies and grew. The size of the microvoids in the W-2%TiC alloy was larger than that in the W-1%TiC alloy with inhomogeneous distribution of TiC nano-particles. The thermal stability of the TiC nano-particles in the W alloys with increasing annealing temperature is shown in Fig. 4, where the CDB ratio curves of annealed W-TiC alloys to pure W fabricated by SPS are also shown. The vertical axis is the ratio of the spectrum of the annealed samples to that of pure W, and all spectra were normalized by the total count. The horizontal axis is the momentum of electrons, m_0c, where m_0 is the electron rest mass, and c is the velocity of light. To dentify the TiC nano-particles, the ratio curve of pure TiC to pure W is also shown in Fig. 4. The ratio curve of the pure TiC showed a shallow valley at $\sim 25 \times 10^{-3}\ m_0c$. The ratio curves of the W-1%TiC alloy were largely unchanged upon annealing at 100–1000 °C. Similarly, the ratio curves of the W-2%TiC alloy did not change even when the annealing temperature was increased to 900 °C. However, the ratio curve of the W-2%TiC alloy annealed at 1000 °C was different from those of the alloys annealed at lower temperatures. The cause of the increase in the value of the high-momentum region of CDB spectrum annealed at 1000 °C is not a decrease in the value of the low-momentum region. This indicated that the TiC nano-particles grew during annealing at 1000 °C, although significant growth of TiC nano-particles was not observed by SEM. It has been reported that vacancies induced by irradiation promote the formation of Cu precipitates in Fe [13]. Therefore, it is possible that the vacancies induced by the alloy fabrication process and thermal treatments also promote the growth of TiC nano-particles in the W alloy.

Fig. 5 shows the microstructures in the W-TiC alloys after He irradiation at 900 °C to 1.8×10^{21} He/m^2. For comparison, the microstructures of the commercial W after He irradiation under the same conditions is also shown in Fig. 5, which have been previously published [14]. The upper section of the figure shows the microstructures in W-1%TiC and the lower part shows the microstructures in W-2%TiC and commercial W. The left section shows the microstructures in the unirradiated samples, and the right part shows the microstructures in the irradiated samples. Only dislocations that were induced during the alloy fabrication process were observed in the as- received W–TiC alloys. He bubbles were observed in all samples after He irradiation at 900 °C to 1.8×10^{21} He/m^2. The formation of He bubbles was suppressed, despite the difference in the magnification of the images, indicating that the size of the He bubbles decreased in the W–TiC alloys compared with that in commercial W. This trend became more significant as the amount of TiC nano-particles increased. The mechanism underlying the suppression of formation of He bubbles in the W-TiC alloys is believed to be due to TiC nano-particles trapping the vacancies

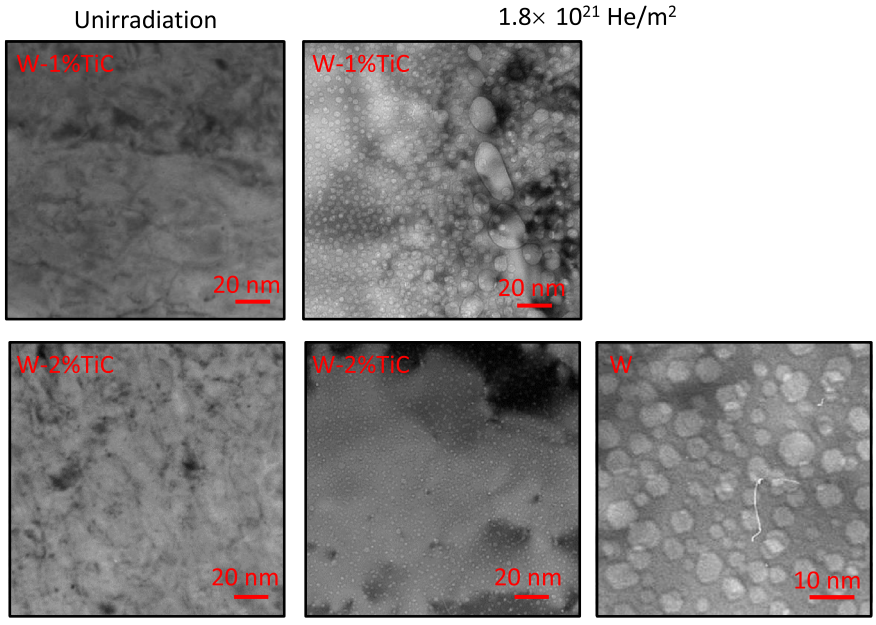

Fig. 5. TEM observation of the microstructures in W–TiC alloys and commercial W irradiated with 5 keV He at 900 °C using an ion accelerator-TEM system.

and irradiation-induced He. This trapping effect becomes more prominent as the amount of TiC nano-particles in the alloy increases. Unfortunately, the distribution of He bubbles in the W-1%TiC alloy was not uniform, indicating that the distribution of TiC nano-particles, too, was not uniform in W-1%TiC. Therefore, it is necessary to improve the manufacturing process for the W-1%TiC alloy to achieve a more uniform distribution of TiC nano-particles.

4. Conclusion

Two kinds of dispersions of secondary-phase W-TiC alloys were developed using SPS. The TiC nano-particles were thermally stable in the W-1%TiC and W-2%TiC alloys even when annealed at temperatures up to 1000 °C for 5 h. The TiC nano-particles significantly suppressed the formation of He bubbles, and this suppression became more prominent as the amount of TiC nano-particles in the alloy increased.

Acknowledgments

This work was partially supported by a Grant-in-Aid for Scientific Research of the Ministry of Education, Science and Culture, under contract No. 15K06423, and partially performed with the support and under the auspices of the NIFS Collaboration Research Program (NIFS17KLPF055).

Supplementary materials

Supplementary material associated with this article can be found, in the online version, at doi:10.1016/j.nme.2018.02.003.

References

[1] H. Kurishita, S. Matsuo, H. Arakawa, T. Sakamoto, S. Kobayashi, K. Nakai, T. Takida, M. Kato, M. Kawai, N. Yoshida, J. Nucl. Mater. 398 (2010) 87–92.
[2] H. Kurishita, S. Kobayashi, K. Nakai, T. Ogawa, A. Hasegawa, K. Abe, H. Arakawa, S. Matsuo, T. Takida, K. Takebe, M. Kawai, N. Yoshida, J. Nucl. Mater. 377 (2008) 34–40.
[3] H. Kurishita, Y. Amano, S. Kobayashi, K. Nakai, H. Arakawa, Y. Hiraoka, T. Takida, K. Takebe, H. Matsui, J. Nucl. Mater. 367–370 (2007) 1453–1457.
[4] S.T. Lang, Q.Z. Yan, N.B. Sun, X.X. Zhang, C.C. Ge, Fusion Eng. Des. 121 (2017) 366–372.
[5] X.Y. Ding, L.M. Luo, H.Y. Chen, G.N. Luo, X.Y. Zhu, X. Zan, J.G. Cheng, Y.C. Wu, Fusion Eng. Des. 92 (2015) 29–34.
[6] L.M. Luo, X.Y. Tan, H.Y. Chen, G.N. Luo, X.Y. Zhu, J.G. Cheng, Y.C. Wu, Powder Technol. 273 (2015) 8–12.
[7] I. Wesemann, W. Spielmann, P. Heel, A. Hoffmann, Int. J. Refract. Met. Hard Mater. 28 (2010) 687–691.
[8] J.F. Ziegler, SRIM-2008, v.2008.40 (2008). Available at <http://www.srim.org>.
[9] T. Troev, E. Popov, N. Nankov, T. Yoshiie, J. Phys. C 207 (2010) 012033.
[10] E. Kuramoto, T. Tsutsumi, K. Ueno, M. Ohmura, Y. Kamimura, Comp. Mater. Sci. 14 (1998) 28–35.
[11] Q. Xu, T. Yoshiie, H.C. Huang, Nucl. Instrum. Meth. B 206 (2003) 123–126.
[12] G.D. Samolyuk, Y.N. Osetsky, R.E. Stoller, Fusion Sci. Technol. 71 (2017) 52–59.
[13] Q. Xu, T. Yoshiie, K. Sato, Phys. Rev. B 73 (2006) 134115.
[14] Q. Xu, X.Y. Ding, L.M. Luo, M. Miyamoto, M. Tokitani, J. Zhang, Y.C. Wu, J. Nucl. Mater. 496 (2017) 227–233.